APL Materials

RESEARCH ARTICLE | DECEMBER 21 2023

Effects of elevated-temperature deposition on the atomic structure of amorphous Ta_2O_5 films

K. Prasai ; K. Lee; B. Baloukas ; H-P. Cheng ; M. Fazio ; L. Martinu; A. Mehta ; C. S. Menoni ; F. Schiettekatte ; R. Shink ; B. Shyam ; G. Vajente ; M. M. Fejer ; R. Bassiri

Check for updates

APL Mater. 11, 121112 (2023)
https://doi.org/10.1063/5.0170100

View Online
Export Citation

29 April 2024 16:29:10

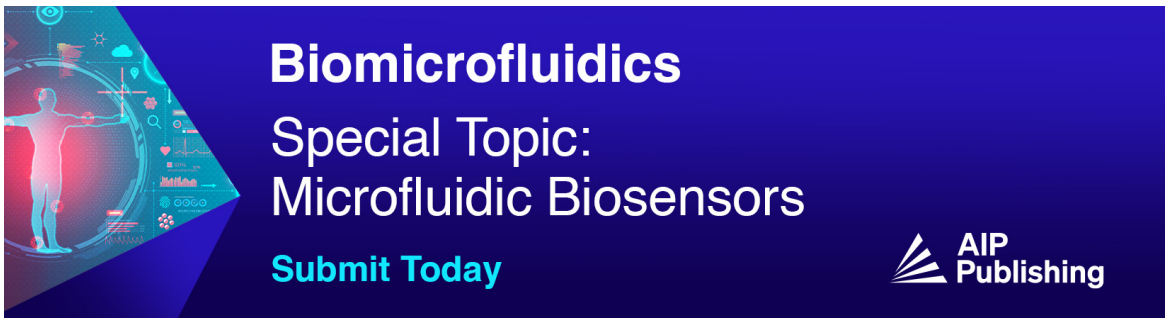

AIP Publishing

Effects of elevated-temperature deposition on the atomic structure of amorphous Ta_2O_5 films

Cite as: APL Mater. 11, 121112 (2023); doi: 10.1063/5.0170100
Submitted: 31 July 2023 • Accepted: 1 December 2023 •
Published Online: 21 December 2023

View Online Export Citation CrossMark

K. Prasai,[1,a)] K. Lee,[2] B. Baloukas,[3] H-P. Cheng,[4] M. Fazio,[5] L. Martinu,[3] A. Mehta,[6] C. S. Menoni,[7] F. Schiettekatte,[8] R. Shink,[8] B. Shyam,[9] G. Vajente,[10] M. M. Fejer,[1] and R. Bassiri[1,b)]

AFFILIATIONS

[1]E. L. Ginzton Laboratory, Stanford University, Stanford, California 94305, USA
[2]Sungkyunkwan University, Seoul 03063, Republic of Korea
[3]École Polytechnique de Montréal, Montréal, Quebec H3T 1J4, Canada
[4]Department of Physics, University of Florida, Gainesville, Florida 32611, USA
[5]SUPA, Department of Biomedical Engineering, University of Strathclyde, Glasgow G1 1QE, United Kingdom
[6]SLAC National Accelerator Laboratory, Menlo Park, California 94025, USA
[7]Department of Electrical and Computer Engineering, Colorado State University, Fort Collins, Colorado 80523, USA
[8]Department of Physics, Université de Montréal, Montréal, Québec H3T 1J4, Canada
[9]Xerion Advanced Battery Corporation, Kettering, Ohio 45420, USA
[10]LIGO Laboratory, California Institute of Technology, Pasadena, California 91125, USA

[a)]**Author to whom correspondence should be addressed:** prasai@stanford.edu
[b)]rbassiri@stanford.edu

29 April 2024 16:29:10

ABSTRACT

Brownian thermal noise as a result of mechanical loss in optical coatings will become the dominant source of noise at the most sensitive frequencies of ground-based gravitational-wave detectors. Experiments found, however, that a candidate material, amorphous Ta_2O_5, is unable to form an ultrastable glass and, consequently, to yield a film with significantly reduced mechanical loss through elevated-temperature deposition alone. X-ray scattering PDF measurements are carried out on films deposited and subsequently annealed at various temperatures. Inverse atomic modeling is used to analyze the short and medium range features in the atomic structure of these films. Furthermore, *in silico* deposition simulations of Ta_2O_5 are carried out at various substrate temperatures and an atomic level analysis of the growth at high temperatures is presented. It is observed that upon elevated-temperature deposition, short range features remain identical, whereas medium range order increases. After annealing, however, both the short and medium range orders of films deposited at different substrate temperatures are nearly identical. A discussion on the surface diffusion and glass transition temperatures indicates that future pursuits of ultrastable low-mechanical-loss films through elevated temperature deposition should focus on materials with a high surface mobility, and/or lower glass transition temperatures in the range of achievable deposition temperatueres.

© 2023 Author(s). All article content, except where otherwise noted, is licensed under a Creative Commons Attribution (CC BY) license (http://creativecommons.org/licenses/by/4.0/). https://doi.org/10.1063/5.0170100

INTRODUCTION

Brownian thermal noise originating from the highly reflective mirror coatings in interferometric gravitational wave detectors (GWDs), such as LIGO and Virgo, forms the primary source of noise within the most sensitive region of the detector signal band (~200 Hz). Future generations of GWDs depend on the mitigation of thermal noise, which can be achieved primarily by employing coatings with lower mechanical loss.[1]

Ongoing research efforts to reduce coating mechanical loss have explored the use of "ultrastable" glasses. In amorphous silicon

© Author(s) 2023

(a-Si), for example, films deposited at progressively higher temperatures up to 400 °C exhibited extremely low mechanical loss (ϕ) at cryogenic temperatures.[2] This behavior is attributed to the structural homogeneity attained by increased surface mobility during deposition at elevated substrate temperatures.[3–5] As a result, the density of the two-level systems (TLS) responsible for mechanical loss is reduced.[6]

The present generation of GWDs utilize dielectric mirror coatings composed of alternating layers of amorphous silica (SiO_2) and titania-doped tantala (Ti:Ta_2O_5).[7,8] It is unclear whether these materials or other amorphous oxides, the main coating material candidates, can be deposited as ultrastable glasses. Prior studies have suggested that properties such as glass transition temperature (T_g), fragility, and surface mobility are pivotal factors in determining whether a material can form an ultrastable glass through elevated-temperature deposition.[5,9,10]

The deposition of amorphous Ta_2O_5 (a-Ta_2O_5) films[11] and more recently of amorphous GeO_2 films[12] at elevated temperatures has produced films that show about a factor of two reduction in mechanical loss over films deposited at ambient temperatures. When these films were subjected to their maximum pre-crystallization post-deposition annealing temperature, a standard process for GWD mirror coatings, the mechanical loss of the films only depended on the annealing temperature and was virtually independent of deposition temperature. This suggests that no significant change to the TLS distribution occurs in these films upon elevated-temperature deposition and that heat treatment erases the deposition thermal history and, therefore, does not form an ultrastable glass. A deeper comprehension at the atomic level that can explain these observations is currently lacking and is the subject of this study.

Here, we report on the effects of elevated-temperature deposition and post-deposition annealing on the atomic structure of films of a-Ta_2O_5. We used x-ray grazing-incidence pair distribution function (GIPDF) measurements to study the local atomic structure of films grown and subsequently annealed at various temperatures. Inverse atomic modeling was then used to analyze the short and medium range features in the atomic structure. Furthermore, *in silico* deposition simulations of a-Ta_2O_5 were carried out at various substrate temperatures, and an atomic level analysis of the deposition at high temperatures is presented. A discussion is then provided to explain why Ta_2O_5 does not and cannot form an ultrastable glass when deposited at elevated temperatures in contrast to, for example, a-Si.[2] We then discuss the implications for achieving lower mechanical loss and, therefore, lower thermal noise coatings.

METHODS

GIPDF measurements

GIPDF measurements were carried out on 1 μm-thick films of a-Ta_2O_5. The films were deposited on 1 mm-thick silica disks using magnetron sputtering with substrates maintained at room temperature (RT), 250, and 400 °C. For GIPDF measurements, two samples deposited at each of the three temperatures were taken; prior to the measurements, one of the two samples was also subjected to post-deposition annealing at 500 °C for 10 h. Further details on the deposition of these films are published in Ref. 11. GIPDF data were collected at the dedicated x-ray scattering beamline 10-2 at the Stanford Synchrotron Radiation Lightsource (SSRL). Using an energy-resolved point detector to scan over the scattering angles, a q-dependent scattering profile was collected for each sample. A grazing incidence angle was chosen such that only x rays scattered from the coatings are collected and not the substrate while maintaining a relatively high q-range of 20.1 Å^{-1}. The elastic signal from the scattered x rays was used to obtain the total scattering signal from the coating, while the fluorescence signal from the tantalum L1, L2, and L3 edges was used as a correction to the detector "foot-print" on the measured intensities. For statistical accuracy, the average of at least six scans was taken across the entire q range for each sample. The total scattering data were reduced to the normalized structure factor [$S(q)$] after applying identical corrections on all samples for air scattering, absorption, Compton scattering, and polarization effects. The structure factors are then Fourier-transformed to r-space to obtain x-ray PDFs for each sample. Further details on the GIPDF data collection method are discussed in Refs. 13 and 14. The x-ray scattering data from the sample deposited at 400 °C and annealed at 500 °C showed signs of substrate contamination due to sample misalignment during data collection, and the data from this sample were excluded from the analysis. We do not consider Ar in this analysis since the Ar content in all samples is <1% and there is no coherent Ar–O or Ar–Ta distances detectable by GIPDFs.

Generating structure models

We generate atomic structure models of a-Ta_2O_5 with a focus on capturing the differences in the measured GIPDFs of the films deposited/annealed at different temperatures. When modeling such data, it is common to choose regression methods, such as simulated annealing (SA[15]) or reverse Monte Carlo (RMC[16]), which fit the atomic coordinates to minimize the differences between the measured PDFs from films and the computed PDFs from models. However, unaided regression algorithms are known to produce nonphysical structure solutions even in elemental systems.[17] In this work, we use the Force Enhanced Atomic Refinement (FEAR) method,[18,19] which takes the approach of iterating a few hundred steps of RMC with a few steps of energy minimization until a convergence in χ^2 and energy is obtained. We define χ^2 as

$$\chi^2 = \sum_j (S_j^{\text{expt}}(q) - S_j^{\text{calc}}(q))/\sigma_j^2, \tag{1}$$

where the sum is over j, which indexes discrete bins in the q-range of interest, and $S^{\text{expt}}(q)$ and $S^{\text{expt}}(q)$ are the experimental and modeled structure factors, respectively. σ is a weighing factor and can be taken as the estimated error in $S^{\text{expt}}(q)$. The energy is calculated using a BKS–Morse potential[20] with parameters proposed by Trinastic *et al.*[21] Starting configurations are generated using the quench-from-the-melt method[17] by carrying out molecular dynamics (MD) simulations. The size of the simulation box is chosen so that the density is 7.51 g/cm^3, which corresponds to the measured density of these films (see Ref. 11) after correcting for Ar and H concentrations. A bond valence sum was added to χ^2 from 1 to make an effective cost function for the RMC. In addition, we constrained each RMC move by requiring that the metal–oxygen bond distances lie in the range of 1.5–3 Å. In the following discussion, these models will be described as "regression models." We find that regression

29 April 2024 16:29:10

© Author(s) 2023

models demonstrate excellent agreement with the measured PDFs. This agreement is enabled by combining RMC and energy minimization using the FEAR method. It is important to note that the models generated by methods using solely unaided BKS potentials, e.g., melt–quench MD simulations, do not have as good agreement with measurements as the regression models presented in this work. The modeling program was instantiated 100 times in parallel, each instance with an independent starting configuration and randomization, resulting in 100 independent atomic models corresponding to each sample. All the properties reported hereafter are averages over those 100 models, and the errors are the corresponding standard deviations.

Vapor deposition simulations

We generate models of vapor deposited a-Ta_2O_5 by following a simulation process that mimics laboratory vapor deposition. We begin by taking a block of melt–quench MD-generated model of a-Ta_2O_5 as substrates—these contain 3500 atoms and have dimensions 50 × 50 Å in the plane perpendicular to the growth direction and are about 19 Å thick along the direction of growth. Following Ref. 4, the atoms on the bottom 1 Å of the substrate are attached to harmonic springs with a spring constant of 0.5 eV/Å^2. The films are grown by injecting atoms within a rectangular volume of space V_{inj} that has dimensions of 50 × 50 × 2 Å and is maintained 4 Å above the free surface along the growth front at all times. The atoms are spawned in a batch of 21 at random positions within V_{inj} while maintaining a minimum distance of 6 Å from each other. In the following discussion, we refer to the set of newly injected atoms as S_{inj} and the set of substrate and the already deposited atoms as S_{film}.

The initial velocities of S_{inj} are randomly initialized to a temperature of T_{inj} following a Maxwell–Boltzmann distribution. Following the injection, a MD simulation is carried out for 50 ps in an NVT ensemble when the temperature of S_{film} is set to T_{sub} at all times, whereas the temperature of S_{inj} is set to T_{inj} for first 10 ps, is gradually reduced to T_{sub} in next 10 ps, and then finally set to T_{sub} for next 30 ps. Then, the energies of atoms are minimized to their local minima using the FIRE algorithm before a fresh batch of atoms are injected. This process is repeated until 22 000 atoms have been deposited on the film. The films are then taken through the MD simulation at 300 K for 10 ps, and a snapshot of atomic configuration is saved every 0.1 ps. For each simulation, the atomic structure calculations are performed and averaged over those saved configurations. Unless otherwise stated, these calculations were performed on a 50 × 50 × 50 Å block that is roughly equidistant from the substrate on one side and the free surface on the other.

These *in silico* depositions are carried out for T_{sub} equal to RT, 250, 400, 600, and 800 °C. To obtain the quantities reported, five independent instances of deposition simulations were carried out at each growth temperature. The reported quantities are averages, and the errors are the standard deviations over those five independent instances.

RESULTS AND DISCUSSION

The measured GIPDFs and atomic models described in the section titled Methods are analyzed to identify atomic structure changes as a function of deposition temperature and annealing. The local order in amorphous materials is often described in terms of short range order (SRO) defined as $r < 0.5$ nm and medium range order (MRO) defined as $0.5 < r < 5$ nm.[22] In the following, we discuss SRO and MRO changes in the films based on the analysis of GIPDF data, regression models, and vapor-deposited models.

The measured PDFs, $G(r)$, are shown in Fig. 1 (a). The first observed peak (P_1) in the PDFs corresponds to a Ta–O correlation, at 1.97 Å. The O–O correlation peak lies at around 2.76 Å;[23] however, no peak is observed in the measured PDFs because of the low scattering cross section of O compared to Ta. The Ta–Ta correlation registers a strong second peak at 3.75 Å (P_2), with a notable hump near 3.33 Å (H_2). As has previously been reported,[24] P_2 corresponds to the Ta–Ta correlation between corner-sharing (CS) polyhedra, whereas H_2 corresponds to the edge-sharing (ES) and face-sharing (FS) polyhedra. The most prominent change in SRO appears in the height of P_2 and H_2 [see the inset of Fig. 1(a)]. This implies changes in O-sharing between adjacent Ta-centred polyhedra as a result of elevated-temperature deposition, as discussed later in Fig. 3. After annealing, the SRO of the samples appears mostly identical.

The PDFs of the as-deposited films deposited at RT, 250, and 400 °C show subtle increases in peak height and structure beyond 5 Å in the MRO region. It, therefore, appears that increasing the deposition temperatures increases the MRO. This trend is also apparent in Fig. 1(b), where the first peak of $S(q)$, which is associated with the degree of MRO,[22] is higher for 400 °C deposited films than for lower deposition temperatures. However, upon annealing, the $G(r)$ and $S(q)$ of the RT deposited and 250 °C deposited films are very similar in both SRO and MRO. We find that annealing produces changes in SRO and MRO, but such changes are more pronounced in films deposited at RT [see Fig. 1(c)]. The latter observation appears to support the hypothesis that elevated-temperature deposition at 250 °C produces similar effects on films as does annealing at 500 °C. These results appear to correlate with the metrology measurements reported in Ref. 11, where the mechanical loss is reduced upon elevated-temperature deposition and becomes identical after annealing, suggesting that annealing erases the thermal history of the films.

To probe the subtle changes observed in the measured PDFs, we analyze the regression models that have been generated by directly fitting the structure to measurement data from films. These models allow for the detailed analysis of the atomic structure of each measured film and accurately capture the structure changes in the films as a function of deposition temperature (see Fig. 2) and annealing. In addition, by observing the errors on the modeled $G(r)$ shown in the insets of Fig. 2, we see that most of the observed differences in the PDFs are greater than the error associated with the models.

Previous studies of amorphous zirconia-doped tantala (Zr:Ta_2O_5) observed that films with a lower fraction of edge- and face-shared (ES and FS) polyhedra had lower mechanical loss at room temperature.[24] The percentage of ES and FS-polyhedra computed from the regression models shows that increasing the deposition temperature has produced a slightly lower fraction of ES and FS-polyhedra in films. However, after annealing, the fraction of ES and FS-polyhedra is identical (see Fig. 3). This trend is consistent with the observed trend in mechanical loss.[11] Other SRO features computed from regression models, including coordination numbers of Ta and O and bond-length and bond-angle distributions, are independent of deposition temperature and are not presented.

29 April 2024 16:29:10

© Author(s) 2023

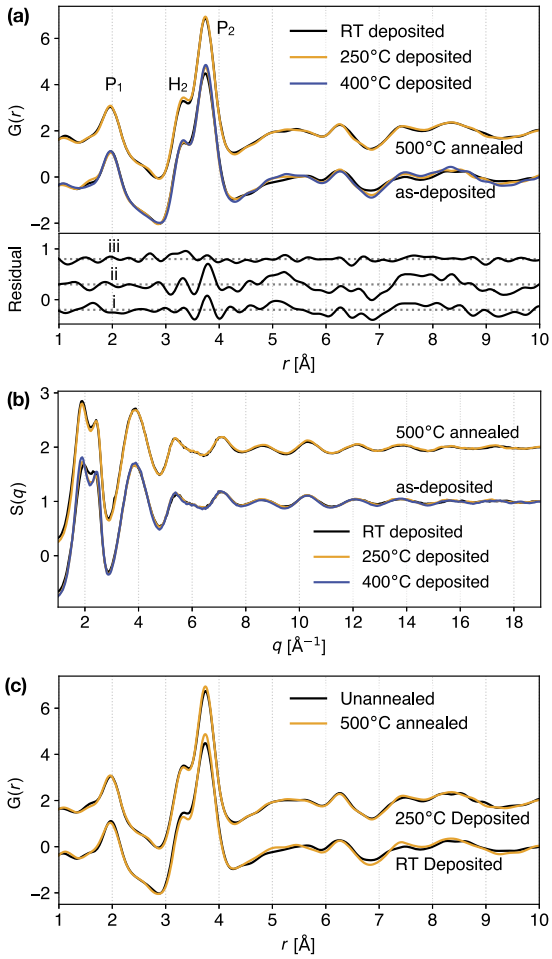

FIG. 1. GIPDF measurement data: (a) G(r) and (b) S(q) of the films plotted for several deposition temperatures, with the 500 °C annealed films shifted along the y-axis; (c) G(r) of the films plotted comparing as-deposited to 500 °C annealed films for two deposition temperatures, with the 250 °C deposited films shifted along the y-axis. The inset of (a) shows the magnified residual of subtraction of G(r)'s. Curve (i) shows the difference between G(r) of as-deposited films deposited at 250 °C and RT. Curve (ii) shows the difference between G(r) of as-deposited films deposited at 400 °C and RT. Curve (iii) shows the difference between G(r) of 500 °C annealed films deposited at 400 °C and RT.

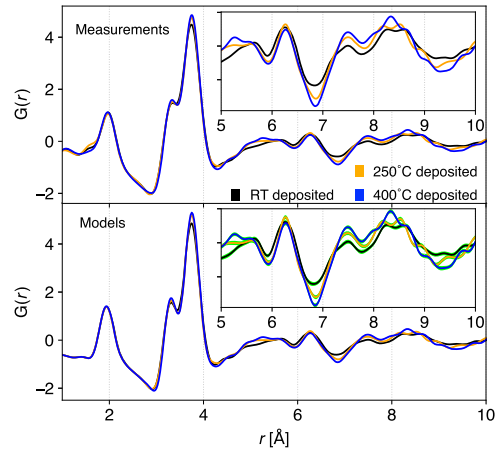

FIG. 2. Ability of atomic models to capture differences observed in the measured GIPDFs as a function of deposition temperature: Top: Measured x-ray PDFs of as-deposited films. Bottom: Computed x-ray PDFs of atomic models fitted to measured S(q) of corresponding films. The insets show the 5–10 Å section (also called the medium range) of PDFs. The green halos around the curves in the inset of the bottom plot represent the estimated error in the PDFs as computed from the standard deviation from 100 independent models.

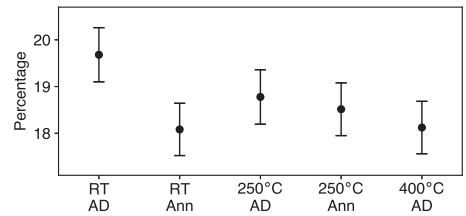

FIG. 3. Edge- and face-sharing polyhedra: Percentage of edge- and face-sharing polyhedra computed from regression models. The tick labels on abscissa indicate the deposition temperature and state of annealing, respectively. "AD" refers to the as-deposited means, and "Ann" refers to annealed at 500 °C.

In Fig. 4, we plot the partial PDFs from the models. The Ta–O correlations show no change as a result of elevated-temperature deposition [Fig. 4(a)], which is unsurprising given the strong chemical bond between Ta and O. The largest change in local order is observed in the MRO upon elevated-temperature deposition in the Ta–Ta correlation [Fig. 4(b)] and is almost identical after annealing regardless of deposition temperature. The change in the Ta–Ta correlation might involve changes in polyhedral connections as discussed previously and also in the evolution of longer range chain structures, as recent modeling data have suggested.[25] Figure 4(c) also shows no change in the O–O correlation, which could be a modeling artifact as this correlation is not well represented in the measured GIPDFs used for the models due to the significantly lower scattering cross section of O compared to Ta.

Simulated vapor deposition offers an alternative approach to study the changes in the atomic structure caused by elevated-temperature deposition. Inexpensive in computation time, such simulations also help identify the deposition parameters (e.g., surface mobility, deposition rate, and particle velocity) that are consequential to the observed changes in the structure. Here, the simulations were carried out with the limited goal of understanding any substrate-temperature-related effect on the structure of the film, as such there are discrepancies between modeled and experimental deposition conditions that are necessary due to achievable computational model sizes and timescales. Such studies have previously identified meaningful predictions when compared to experimental data.[4,26]

For our data, the deposition rate in the simulations was 2.3 $\times 10^9$ Å/s, while the experimental deposition rate was 2.07 Å/s.[11] While the physical films were 1 μm thick, our vapor deposited models are only 12 nm thick. Furthermore, the physical films were

29 April 2024 16:29:10

© Author(s) 2023

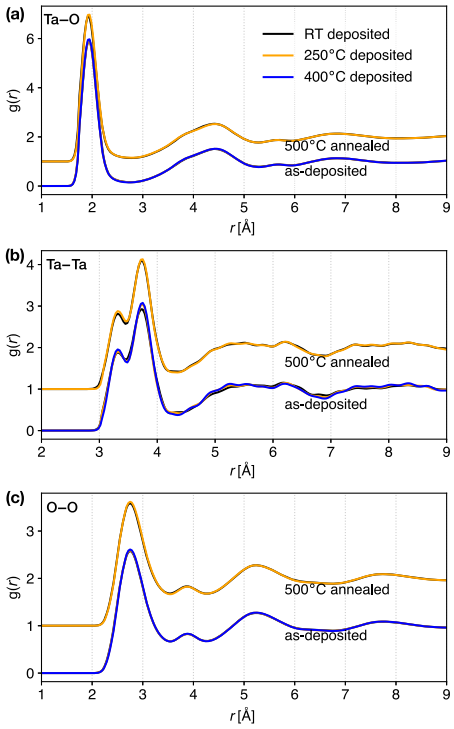

FIG. 4. Partials PDFs: Partial PDFs computed from the regression models. (a)–(c) Show Ta–O, Ta–Ta, and O–O partials, respectively. Partial PDFs of the annealed models are shifted along the vertical axis for clarity.

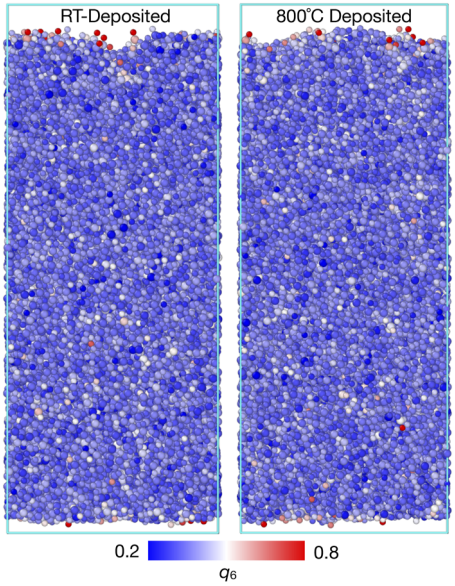

FIG. 5. Vapor deposited models: Graphical representation of models of a-Ta_2O_5 prepared by simulated vapor deposition. The colors of atoms represent the computed bond orientational order parameter, q_6.[28] The distribution of q_6 shows that both RT-deposited and 800 °C-deposited models are fully amorphous.

deposited on silica substrates. Since the simulated films represent the top 12 nm near the surface, it is unlikely to exhibit interface effects due to a silica substrate. Therefore, we model the substrate by attaching harmonic springs to the bottom layer of the melt–quench MD generated models of Ta_2O_5.

Ion-beam-deposited a-Ta_2O_5 films were observed to remain amorphous at a deposition temperature of 500 °C, while magnetron sputtered films deposited at 480 °C showed signs of crystallization.[11] IBS films remain amorphous at an annealing temperature of 600 °C.[11,27] Here, vapor-deposition simulations are carried out at T_{sub} = RT, 250, 400, 600, and 800 °C, and the films remain amorphous. Figure 5 shows the models of the simulated films for T_{sub} equal to RT and 800 °C. The values of q_6 are used for coloring the atoms and demonstrate that the films are fully amorphous at the respective deposition temperatures. The reason for *in silico* vapor deposited models to remain amorphous at higher deposition temperatures than seen in experiments is likely related to the significantly faster deposition rate used in our simulations compared to experiments. Although one can further decrease the deposition rate in simulations, it is computationally impracticable to carry out simulations at experimental deposition rates.

For e-beam deposited amorphous Si films, elevated substrate temperatures during deposition produced films with a higher density and also demonstrated significantly lower mechanical loss, below the standard glass range.[2] In addition, Lennard-Jones models of ultrastable glasses prepared by simulations of deposition at elevated substrate temperatures found that such glasses are significantly denser than ordinary glasses.[4] We, therefore, compute the density of our vapor deposited models to identify any dependence on T_{sub}, and the results are plotted in Fig. 6. The resulting densities are identical or within error for all deposition temperatures and are close to the density of the simulated melt–quench models reported in Ref. 21 (represented by the dotted line). Note that these densities are different from the densities of regression models, which were fixed to 7.51 g/cm^3 taken from experiments.[11] These models also demonstrate no significant density gradient across the thickness as confirmed by the densities computed from selected volumes of models near the substrate, middle, and surface of the modeled films.

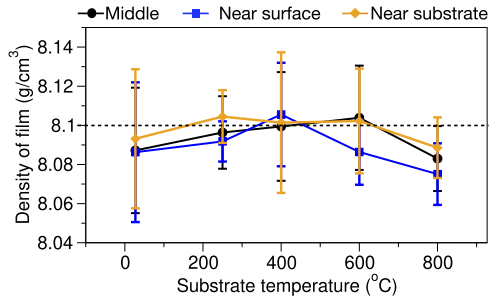

FIG. 6. Densities of modeled films: Average densities of vapor deposited models at each deposition temperature. The error bars indicate the standard deviation. The colors indicate the region of the film where density is computed. The regions are 50 × 50 × 50 Å in dimension and are overlapping. The dotted line represents the density of models from melt–quench MD simulations.[21]

29 April 2024 16:29:10

© Author(s) 2023

Analyzing the SRO of modeled films, we find that the first coordination sphere shows strong structural order. Our analysis tracked coordination around Ta and O atoms and found that these remain unchanged as a function of deposition temperature or are within error (not plotted here). This observation implies that the Ta-centered polyhedra, which are considered the primary building blocks of Ta_2O_5, remain unaffected by elevated-temperature deposition. It is again unsurprising given that the strongest chemical order is expected in the first coordination sphere. Some change in bond-angle distribution between models deposited at RT and 800 °C is observed in Fig. 7(a). For simplicity, we only present the models of films with the greatest contrast in deposition temperature, deposited at RT and 800 °C. Although these changes are beyond the error, they are smaller than what is observed upon annealing. A numerical annealing of a-Ta_2O_5 using the same interatomic potential as in this work and utilizing the population annealing method is presented in Ref. 29. The changes in the bond-angle distribution upon annealing observed in the latter work are greater than that shown in Fig. 7(a). The distribution of bond orientational order parameter, plotted in Fig. 7(b), shows only subtle changes between RT-deposited and 800 °C-deposited. The changes are similar to those observed as a result of annealing in Ref. 29. An interesting trend is observed upon the analysis of Voronoi volumes of the vapor deposited models shown in Fig. 7(c). It suggests that the models deposited at RT have a small number of Voronoi polyhedra with larger than 20 Å^3 volume, and such polyhedra are not present in the models deposited at 800 °C. Larger Voronoi polyhedra are associated with the presence of nanovoids in the network, which could be responsible for some of the differences observed in the MRO.[22] This observation suggests that elevated-temperature deposition results in a more uniform amorphous network.

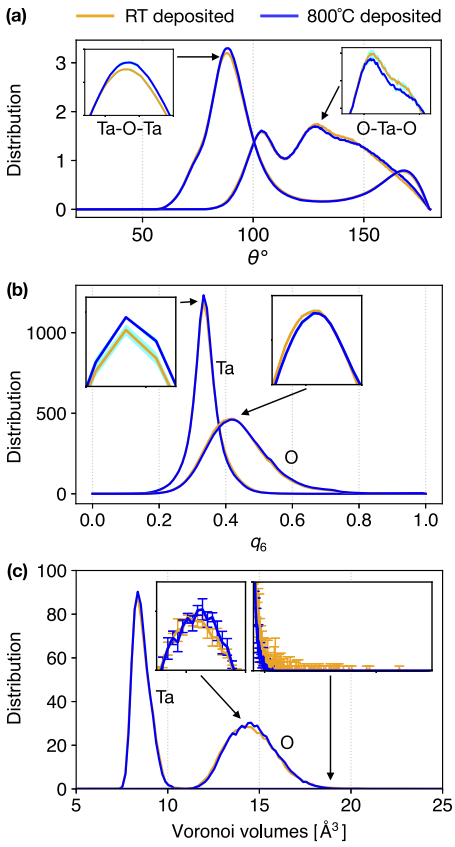

FIG. 7. Short-range structure of vapor deposited models: (a) Bond angle distribution computed from the models deposited at RT and 800 °C. (b) Distribution of bond order orientational parameter q_6 computed from the models deposited at RT and 800 °C. (c) Distribution of Voronoi volumes computed from models deposited at RT and 800 °C.

For a-Ta_2O_5 films, elevated-temperature deposition has only demonstrated relatively small effects on the atomic structure, which appear identical after post-deposition annealing on films deposited at any temperature. These results are in disagreement with observations on, for example, amorphous silicon,[2] indomethacin,[30] and other glasses, where elevated-temperature deposition is known to produce films with structures and properties that RT deposition and subsequent annealing cannot. Many studies have suggested the role of the mobility of surface atoms—that in some materials, surface atoms are significantly more mobile than bulk atoms and elevated-temperature deposition allows these materials to organize into a stable structure—which cannot be achieved through annealing alone. This implies that future pursuits of low mechanical loss coatings should focus on materials with higher surface mobility.[31]

We attempted to calculate the surface and bulk diffusion coefficients for a-Si and obtained results that were on par with earlier theoretical studies,[32,33] however these were several orders of magnitude higher than previous measurements of diffusion coefficients.[34] Our calculations on Ta_2O_5 demonstrated a surface diffusion that was around two times less than a-Si, however due to the large discrepancy between theoretical and measured mobility coefficients in a-Si, we cannot reliably draw conclusions from our calculations. It appears that the atomic level mechanism(s) behind the difference in mobility between a-Si and a-Ta_2O_5 cannot be fully captured by current simulation techniques and will therefore be the subject of future investigations.

Furthermore, the theoretical T_g of Si is estimated to be close to 730 °C,[37] while that of Ta_2O_5 is estimated to be ~1250 °C.[38] Taking the optimal substrate temperature for achieving ultrastable effects to be 0.8 T_g,[4] such a temperature is much lower for a-Si than for a-Ta_2O_5. 0.8 T_g of Ta_2O_5 is ~945 °C, and attempts to deposit at such high temperatures are challenging and will likely lead to crystallization well below 0.8 T_g.[11]

CONCLUSIONS

The effect of elevated-temperature deposition and annealing on the atomic structure of films of a-Ta_2O_5 was studied using GIPDF measurements and regression-based modeling. An analysis of the measured PDFs and subsequent atomic models of Ta_2O_5 was carried out. It was observed that films deposited at 250 and 400 °C show increased order beyond the first coordination sphere (< 2.8 Å) and in MRO. However, upon annealing at 500 °C, the structures of the films are largely identical irrespective of the deposition temperature of the films. These results mirror the previously reported trends observed in the measured mechanical loss where elevated-temperature deposition did not yield lower mechanical losses than can be achieved by post-deposition annealing alone.[11]

29 April 2024 16:29:10

© Author(s) 2023

Models were also obtained after simulated vapor deposition with substrates maintained at RT, 250, 400, 600, and 800 °C. These models show largely identical structures with respect to the substrate temperature during deposition—with only small changes in bond angles and q_6 distributions and the pruning of O-centred Voronoi polyhedra larger than 20 Å^3 with higher substrate depositions. This lack of observable difference in the modelled structures could be explained due to Ta_2O_5 having lower surface mobility and/or an achievable deposition temperature, prior to the onset of crystalization, which is well below the $0.8T_g$ required for achieving ultrastability. Therefore, the intended surface rearrangement in Ta_2O_5 cannot be realized and an ultrastable coating with low mechanical loss is not formed.

Given the aim of reduced thermal noise coatings for future GWDs and the limitations of amorphous Ta_2O_5 revealed in our study, future research should pivot toward materials with a higher surface mobility and/or lower glass transition temperatures for the production of ultrastable, low-mechanical-loss, and, therefore, lower thermal noise coatings.

ACKNOWLEDGMENTS

We would like to thank Dr. Beverly Berger for helpful comments in reviewing this article. We acknowledge the support of the LSC Center for Coatings Research, jointly funded by the National Science Foundation (NSF) and the Gordon and Betty Moore Foundation (GBMF). In particular, the authors are grateful for the support through NSF under Award Nos. PHY-2011571, PHY-2011706, and PHY-2011782 and GBMF under Grant No. 6793. Partial support from the Office of Naval Research (ONR) under Grant No. N000-17-1-2536 is acknowledged. We would like to acknowledge the Sherlock Cluster at Stanford University for providing computational resources and support that contributed to these research results. This work also used the Extreme Science and Engineering Discovery Environment (XSEDE),[39] which is supported by the NSF under Award No. ACI-1548562. Authors from U. Montréal and Polytechnique Montréal wish to acknowledge the NSERC, the FRQNT through the RQMP, and the FCI for funding. Authors from Sungkyunkwan Univ. were supported by the National Research Foundation of Korea (NRF) grant funded by the Korean government (MSIT) (Grant No. 2021R1C1C1009248). This paper has LIGO document under Grant No. P2300147.

AUTHOR DECLARATIONS

Conflict of Interest

The authors have no conflicts to disclose.

Author Contributions

K. Prasai: Conceptualization (lead); Data curation (lead); Formal analysis (lead); Funding acquisition (supporting); Investigation (lead); Methodology (lead); Resources (supporting); Software (lead); Validation (lead); Visualization (lead); Writing – original draft (lead); Writing – review & editing (lead). **K. Lee**: Investigation (supporting); Writing – review & editing (supporting). **B. Baloukas**: Resources (supporting); Writing – review & editing (supporting). **H.-P. Cheng**: Funding acquisition (equal); Methodology (supporting); Supervision (supporting); Writing – review & editing (supporting). **M. Fazio**: Data curation (equal); Formal analysis (supporting); Investigation (equal); Writing – review & editing (equal). **L. Martinu**: Resources (supporting); Writing – review & editing (supporting). **A. Mehta**: Conceptualization (supporting); Data curation (supporting); Formal analysis (supporting); Investigation (supporting); Methodology (equal); Resources (equal); Writing – review & editing (supporting). **C. S. Menoni**: Funding acquisition (equal); Resources (equal); Writing – review & editing (equal). **F. Schiettekatte**: Resources (equal); Writing – review & editing (equal). **R. Shink**: Resources (supporting); Writing – review & editing (supporting). **B. Shyam**: Conceptualization (supporting); Data curation (equal); Formal analysis (equal); Investigation (equal); Methodology (equal); Writing – review & editing (equal). **G. Vajente**: Data curation (supporting); Formal analysis (supporting); Investigation (supporting); Resources (supporting); Writing – review & editing (supporting). **M. M. Fejer**: Conceptualization (equal); Funding acquisition (lead); Project administration (equal); Resources (equal); Supervision (lead); Writing – review & editing (equal). **R. Bassiri**: Conceptualization (equal); Data curation (equal); Formal analysis (equal); Funding acquisition (equal); Investigation (equal); Methodology (equal); Project administration (lead); Resources (equal); Supervision (lead); Validation (equal); Visualization (equal); Writing – original draft (equal); Writing – review & editing (equal).

DATA AVAILABILITY

The data that support the findings of this study are available from the corresponding author upon reasonable request.

REFERENCES

[1] J. Steinlechner, Philos. Trans. R. Soc., A **376**, 20170282 (2018).
[2] X. Liu, D. R. Queen, T. H. Metcalf, J. E. Karel, and F. Hellman, Phys. Rev. Lett. **113**, 025503 (2014).
[3] L. Zhu and L. Yu, Chem. Phys. Lett. **499**, 62 (2010).
[4] S. Singh, M. D. Ediger, and J. J. De Pablo, Nat. Mater. **12**, 139 (2013).
[5] L. Berthier, P. Charbonneau, E. Flenner, and F. Zamponi, Phys. Rev. Lett. **119**, 188002 (2017).
[6] D. Khomenko, C. Scalliet, L. Berthier, D. R. Reichman, and F. Zamponi, Phys. Rev. Lett. **124**, 225901 (2020).
[7] B. P. Abbott, R. Abbott, T. Abbott, M. Abernathy, F. Acernese, K. Ackley, C. Adams, T. Adams, P. Addesso, R. Adhikari *et al.*, Phys. Rev. Lett. **116**, 061102 (2016).
[8] G. M. Harry, M. R. Abernathy, A. E. Becerra-Toledo, H. Armandula, E. Black, K. Dooley, M. Eichenfield, C. Nwabugwu, A. Villar, D. Crooks *et al.*, Classical Quantum Gravity **24**, 405 (2006).
[9] A. Sepúlveda, M. Tylinski, A. Guiseppi-Elie, R. Richert, and M. Ediger, Phys. Rev. Lett. **113**, 045901 (2014).
[10] J. H. Mangalara, M. D. Marvin, and D. S. Simmons, J. Phys. Chem. B **120**, 4861 (2016).
[11] G. Vajente, R. Birney, A. Ananyeva, S. Angelova, R. Asselin, B. Baloukas, R. Bassiri, G. Billingsley, M. Fejer, D. Gibson *et al.*, Classical Quantum Gravity **35**, 075001 (2018).
[12] L. Yang, G. Vajente, M. Fazio, A. Ananyeva, G. Billingsley, A. Markosyan, R. Bassiri, K. Prasai, M. M. Fejer, M. Chicoine *et al.*, Sci. Adv. **7**, eabh1117 (2021).
[13] B. Shyam, K. H. Stone, R. Bassiri, M. M. Fejer, M. F. Toney, and A. Mehta, Sci. Rep. **6**, 1 (2016).

29 April 2024 16:29:10

© Author(s) 2023

[14]X. Qiu, J. W. Thompson, and S. J. Billinge, J. Appl. Crystallogr. **37**, 678 (2004).
[15]S. Kirkpatrick, C. D. Gelatt Jr., and M. P. Vecchi, Science **220**, 671 (1983).
[16]D. Keen and R. McGreevy, Nature **344**, 423 (1990).
[17]D. Drabold, Eur. Phys. J. B **68**, 1 (2009).
[18]A. Pandey, P. Biswas, and D. Drabold, Phys. Rev. B **92**, 155205 (2015).
[19]A. Pandey, P. Biswas, and D. A. Drabold, Sci. Rep. **6**, 33731 (2016).
[20]B. Van Beest, G. J. Kramer, and R. Van Santen, Phys. Rev. Lett. **64**, 1955 (1990).
[21]J. Trinastic, R. Hamdan, Y. Wu, L. Zhang, and H.-P. Cheng, J. Chem. Phys. **139**, 154506 (2013).
[22]S. R. Elliott, Nature **354**, 445 (1991).
[23]T. Damart, E. Coillet, A. Tanguy, and D. Rodney, J. Appl. Phys. **119**, 175106 (2016).
[24]K. Prasai, J. Jiang, A. Mishkin, B. Shyam, S. Angelova, R. Birney, D. Drabold, M. Fazio, E. Gustafson, G. Harry *et al.*, Phys. Rev. Lett. **123**, 045501 (2019).
[25]A. Mishkin, J. Jiang, R. Zhang, H.-P. Cheng, K. Prasai, R. Bassiri, and M. Fejer, "Hidden structure in the medium-range order of amorphous zirconia-tantala films," Phys. Rev. B **108**(5), 054103 (2023).
[26]M. A. Caro, V. L. Deringer, J. Koskinen, T. Laurila, and G. Csányi, Phys. Rev. Lett. **120**, 166101 (2018).
[27]M. A. Fazio, G. Vajente, L. Yang, A. Ananyeva, and C. S. Menoni, Phys. Rev. D **105**, 102008 (2022).
[28]P. J. Steinhardt, D. R. Nelson, and M. Ronchetti, Phys. Rev. B **28**, 784 (1983).
[29]K. Prasai, R. Bassiri, H.-P. Cheng, and M. M. Fejer, Phys. Status Solidi B **258**, 2000519 (2021).
[30]T. Pérez-Castañeda, C. Rodríguez-Tinoco, J. Rodríguez-Viejo, and M. A. Ramos, Proc. Natl. Acad. Sci. U. S. A. **111**, 11275 (2014).
[31]Y. Li, A. Annamareddy, D. Morgan, Z. Yu, B. Wang, C. Cao, J. H. Perepezko, M. Ediger, P. M. Voyles, and L. Yu, Phys. Rev. Lett. **128**, 075501 (2022).
[32]S. Sastry and C. Austen Angell, Nat. Mater. **2**, 739–743 (2003).
[33]I. Santos, L. A. Marqués, L. Pelaz, and L. Colombo, Phys. Rev. B **83**, 153201 (2011).
[34]J. Kirschbaum, T. Teuber, A. Donner, M. Radek, D. Bougeard, R. Böttger, J. L. Hansen, A. N. Larsen, M. Posselt, and H. Bracht, Phys. Rev. Lett. **120**, 225902 (2018).
[35]M. P. Allen and D. J. Tildesley, *Computer Simulation of Liquids* (Oxford University Press, 2017).
[36]J. Tersoff, Phys. Rev. Lett. **56**, 632 (1986).
[37]A. Hedler, S. L. Klaumünzer, and W. Wesch, Nat. Mater. **3**, 804 (2004).
[38]K. Prasai, R. Bassiri, H.-P. Cheng, and M. M. Fejer, APL Mater. **11**, 081113 (2023).
[39]J. Towns, T. Cockerill, M. Dahan, I. Foster, K. Gaither, A. Grimshaw, V. Hazlewood, S. Lathrop, D. Lifka, G. D. Peterson, R. Roskies, J. R. Scott, and N. Wilkins-Diehr, Comput. Sci. Eng. **16**, 62 (2014).

29 April 2024 16:29:10

© Author(s) 2023